Experimental evidence of multiple equilibria

in a tidal resonator

By G U I D O M. T E R R A[1,2]†,
W I L L E M J A N V A N D E B E R G[1,3],
and L E O R. M. M A A S[1]

[1]Royal Netherlands Institute for Sea Research, Physics Department, P.O. Box 59, NL-1790 AB
Den Burg, The Netherlands.

[2]Korteweg-de Vries Institute for Mathematics, University of Amsterdam, Plantage
Muidergracht 24, NL-1018 TV Amsterdam, The Netherlands.

[3]Institute for Marine and Atmospheric research Utrecht, P.O. Box 80000, NL-3508 TA
Utrecht, The Netherlands.

Laboratory experiments have been performed with a laboratory tank to study the Helmholtz response of a semi-enclosed tidal basin co-oscillating with an adjacent sea. As opposed to the well-known effect of distortion of the tidal curve due to the generation of overtides, we focus on nonlinear effects on the response curve, amplification factor and tidal difference between basin and sea as a function of forcing frequency and amplitude. Motivated by earlier model studies, the aim of this work is to investigate whether for specific parameter settings nonlinear processes result in the possibility of multiple tidal regimes in the basin: different responses in the basin under the same forcing conditions at sea, the actual state of the basin depending on initial conditions c.q. its history. Consequently, sudden regime changes may occur, even in a chaotic fashion according to model studies. A number of different physical mechanisms have been identified to lead to the same generic behaviour, among which non-uniform hypsometry (if the basin area depends on tidal phase),

† Author to whom correspondence should be addressed: `terra@nioz.nl`.

advective accelerations and the feedback of water level changes on depth-averaged mass flux. The main conclusion of this paper is that, although non-uniform hypsometry is not significant at the laboratory scale, multiple equilibria do occur with a crucial role played by the shape of the inlet between basin and sea. The precise nature of the physical mechanism responsible for the observed effect is still open to further research and a discussion of possible mechanisms is included.

---

1. Introduction

Although direct tidal forcing by the gravitational forces from the moon and the sun is relatively weak (0.27 m, 0.13 m amplitude respectively), tidal motion up to 8 m (Bay of Fundy) amplitude occurs due to resonance in coastal basins co-oscillating with an adjacent sea. This resonance phenomenon is successfully explained with linear models (reviewed in e.g. Defant 1961; Raichlen 1966; LeBlond & Mysak 1978) which provide us with response curves (amplification of the tide as a function of forcing frequency) of particular tidal basins.

Nonlinear effects arise due to many mechanisms, such as advective acceleration, water level feedback on mass fluxes, non-uniform hypsometry (dependence of basin area on the water level as in the case of tidal flats) and quadratic friction. In observational studies nonlinear effects manifest themselves in the generation of higher harmonics (Gallagher & Munk 1971; Parker 1991*b*) distorting the tidal curve from purely sinusoidal to an asymmetric curve. However, from a dynamical systems point-of-view nonlinear terms may also cause more complex behaviour. Indeed, there have been reports of drifting harmonic 'constants' (Doodson 1924; Gutiérrez *et al.* 1981) and even chaotic tidal behaviour (Vittori

1992; Frison *et al.* 1999). In this paper the focus is on changes in a basin's response curve.

An almost enclosed basin, which is connected to an adjacent sea through a narrow inlet only, constitutes a fairly simple example of a tidal resonator. The first eigenmode of such a basin is almost uniform within the basin since its tidal wavelength is much larger than the dimensions of the basin. As such, this so-called *Helmholtz mode* can be described by an ordinary differential equation for the water level inside the basin. Miles (1981) extended his linear theory for the Helmholtz mode (Miles 1971) to include the effect of changing channel cross section with sealevel. This shortens the high water period and increases the low water period. Moreover, the total period of free oscillations increases with amplitude and the response curve is tilted. As a result *multiple equilibria* are found: for the same tidal signal at sea, different tidal response amplitudes in the basin are possible. Consequently hysteresis may occur under changing exterior conditions. Elaborating upon the work of Green (1992), it was shown that non-uniform hypsometry has a similar but opposite effect on the tidal response: reduction of the low water period and lengthening of the high water period (Maas 1997). In the limit of small friction and near resonance, he found multiple equilibria as well. Moreover, if the tidal signal at sea is not purely sinusoidal but consists of a couple of nearly resonant components (such as M_2 and S_2, causing the spring-neap tidal cycle) chaotic behaviour of the response amplitude was shown to occur (Maas & Doelman 2002; Doelman *et al.* 2002). By performing a similar weakly nonlinear analysis on the depth-averaged shallow water equations, their results can be shown to apply to more general basins as well and not restricted to Helmholtz basins with non-uniform hypsometry (Terra *et al.* 2004*b*). In that case the nonlinear effects stem from advective acceleration and water level feedback on mass fluxes. In fact, many nonlinear mechanisms lead to the same weakly nonlinear results.

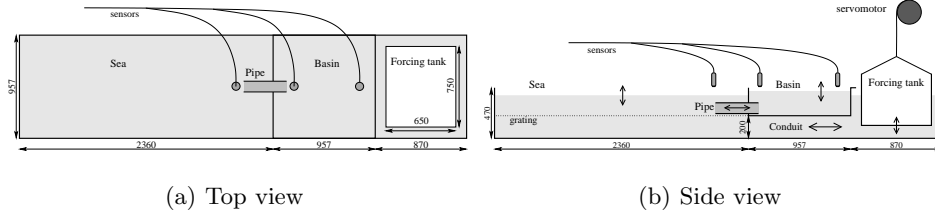(a) Top view   (b) Side view

FIGURE 1. Sketch of the experimental setup, dimensions in mm are indicated. The forcing tank is set into motion by a servomotor. The water expelled by the tank moves through the conduit underneath the 'basin' area to the 'sea'. The tidal signal thus generated at sea, propagates into the basin through a completely submerged pipe. The water level elevation is measured by acoustic sensors at different positions. The sensor positions indicated in the figure represent the standard configuration. Because the tide in the basin is nearly uniform, the measurements for the sensors in the basin are virtually the same.

The occurrence of multiple equilibria is a key ingredient in this route to chaos. This paper describes experiments that have been performed in order to find multiple equilibria in a real (though on a small experimental scale) tidal resonator of the Helmholtz type.

The experimental setup is described in section 2. Although the present work was originally motivated by the results on the effect of hypsometry in Helmholtz basins, the weakly nonlinear results appear to be of generic nature applicable to several nonlinear physical mechanisms. Still, the introduction to the theory in section 3 is restricted to the relatively simple Helmholtz case in which hypsometry is causing nonlinear effects. Discussion of other physical mechanisms that may lead to the same phenomena is postponed until section 5, after having described the experimental results in section 4.

2. Experimental setup

A sketch of our experimental setup is shown in Fig. 1. The area of interest is the 'basin' with a size of 957×957 mm. A completely submerged pipe is used to connect the basin to the forcing tide at 'sea'. In this way, its cross section O does not depend on water level

elevation ζ, in contrast to an open channel which would introduce additional nonlinear effects (Miles 1981). A number of different pipes have been used, with lengths between 300 and 550 mm and diameters of 75–95 mm. The water depth at rest ranged 15–22 cm above the bottom of the basin, making sure that the pipe remained completely submerged, in which case it has no influence the measurements. A forcing tank is immersed in the water and is lifted and lowered by a properly counterbalanced servomotor. The control signal can be generated by the computer. The applied forcing frequencies varied from 0.02 Hz to 0.25 Hz. In principle the forcing signal may consist of many frequency components, but harmonic forcing only is considered in this paper. The water expelled by the forcing tank, moves through the conduit underneath the basin area towards the sea. A grating was inserted in order to help the water level rise at sea to be uniform, but it did not prevent the occurrence of a standing wave: depending on the forcing frequency, amplitudes are higher at the far end of the sea. The amplitude of the control signal is adjusted to obtain the desired forcing amplitude at the mouth of the basin (cf. the discussion at the end of this section), so this has no influence on the measurements. Acoustic sensors are used for nonintrusive measurements of water level elevation. They are located above the tank and emit an acoustic signal at 300 kHz down to the water surface and measure the return time of the reflected signal, like an echo sounder. Their resolution is 0.36 mm, the standard deviation of the noise is similar. Significant outliers occur and were dismissed from the analysis if they differ by more than 3.5 times the standard deviation from a harmonic fit to the time series.

Figure 2 shows time series of laboratory experiments using the full basin area ($A_0 = 0.916$ m^2), a straight pipe ($L = 441$ mm long) with circular cross section ($O = 4.6 \cdot 10^{-3}$ m^2). At least at three locations the water level was measured, above the seaward and basin end of the pipe and at the end of the basin. In correspondence with a Helmholtz
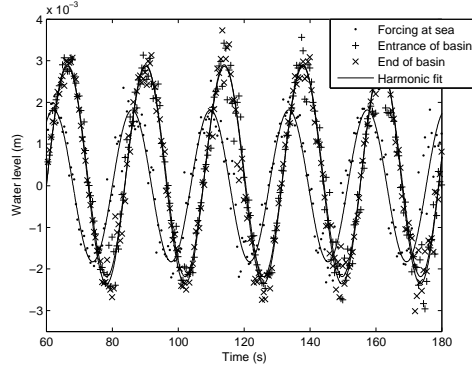
FIGURE 2. Sample time series of measurements at forcing frequency 0.0420 Hz and forcing amplitude approximately 2 mm, for uniform hypsometry with $A_0 = 0.916 \text{ m}^2, L = 441 \text{ mm}, O = 4.6 \cdot 10^{-3} \text{ m}^2$. Dots indicate measurements from the sensor at the seaward pipe entrance, pluses and crosses indicate measurements at the entrance and end of the basin, respectively. Solid curves show harmonic fits to the respective time series. The two curves inside the basin are nearly indistinguishable, consistent with a Helmholtz mode of uniform basin tide.

mode inside the basin the water level was found to be almost uniform. Although the amplitude is usually somewhat higher at the end of the basin, the phases correspond very well. The time series were analyzed by performing a harmonic fit with the dominant frequencies, determined from the Fourier power spectrum. Response curves are determined by comparing the amplitudes and phases of the forcing frequency component both for the sensor at sea and inside the basin.

No dissipators have been installed at the sidewalls of the sea. Raichlen & Ippen (1965) warn that consequent reflections have a dramatic effect on the response curves (amplification factor and phase difference between response in the basin and forcing at sea as a function of forcing frequency). They define the amplification factor as the ratio of the tidal response amplitude in the basin over the amplitude at the seaward entrance *if the basin were closed*. Indeed, radiation damping effects changing the actual tidal signal at

the seaward entrance, are quite different in a finite reflective sea than in a semi-infinite reflectionless sea. We however choose to correct the motion of the forcing tank such that the amplitude at the seaward entrance is the same for all frequencies and define the amplification factor as the ratio of the response amplitude in the basin over the amplitude at sea *with the basin connected to it*. This boils down to eliminating the effect of radiation damping and circumvents the problems mentioned by Raichlen & Ippen (1965).

3. Theory

By considering the momentum and mass balance a simple model can be derived describing the Helmholtz mode of a basin, the dimensions of which are assumed to be much smaller than the tidal wavelength $\lambda = 2\pi\sqrt{gH}/\omega$ (where g is the gravitational acceleration, H the water depth at rest and ω the angular forcing frequency). In that case the water level in the basin will rise and fall almost uniformly and can be described by a single parameter ζ, the elevation relative to the still water level. Water flows into the basin through the pipe of length L, cross section O, into the basin with horizontal area A. In the case of non-uniform hypsometry $A = A(\zeta)$ depends on the water level: at low tide the wet area is less than at high tide when tidal flats are flooded. All dynamics are concentrated in the connecting pipe, where the elevation difference between sea and basin drives the flow, balanced by the inertia of the water in the channel and dissipation by friction/flow separation. Bottom friction is commonly described by Chezy's law $(c_D/H)\,|u|u$, with drag coefficient $c_D \approx 0.0025$ determined empirically (Parker 1991*a*). The head loss due to flow separation is parameterized by $(f/L)\,|u|u$ (Hayashi *et al.* 1966; Terrett *et al.* 1968; Mei *et al.* 1974; Maas 1997) and differs only in the formulation of the coefficient; f has to be determined empirically as well. For our configuration $f \approx 1$ appears to be a good estimate (cf. Terra *et al.* 2004*a*, or section 4.1 of this paper). The

equations for the momentum and mass balance read:

$$\frac{\mathrm{d}u}{\mathrm{d}t} = \frac{g}{L}\,(\zeta_e - \zeta) - \frac{\tilde{f}}{L}\,|u|\,u, \qquad (3.1a)$$

$$A(\zeta)\,\frac{\mathrm{d}\zeta}{\mathrm{d}t} = O\,u, \qquad (3.1b)$$

where $\zeta_e = \alpha_e \cos(\omega t) = \mathrm{Re}[\alpha_e\,\mathrm{e}^{\mathrm{i}\omega t}]$ is the prescribed elevation at sea. The head loss coefficient $\tilde{f}/L$ is considered to include friction with sidewalls as well ($\tilde{f}/L = f/L + c_D/H$, where "$H$" should be related to the radius of the pipe). Head loss due to flow separation seems to be more important here. As in the experiment radiation damping is not modelled here explicitly but is assumed to be already incorporated in ζ_e. In analyzing the experimental results we will also compare the measurements inside the basin with the forcing signal at sea as it is measured simultaneously.

In section 3.1 the Helmholtz model (3.1) with uniform hypsometry ($A(\zeta) = A_0$ independent of ζ) ~~when~~ friction is the only nonlinear term will be dealt with by Lorentz' linearization procedure. In section 3.2 the strong resonance limit for weak friction and forcing frequency ω close to the eigen- (Helmholtz) frequency $\omega_0 = \sqrt{gO/(A_0L)}$ is investigated for linearized friction. The nonlinear effect of non-uniform hypsometry is used to illustrate the generic results of the weakly nonlinear analysis (Doelman *et al.* 2002; Terra *et al.* 2004b) in a simple way. Finally, the two are combined to obtain a correction to the quasi-linear theory from section 3.1 consistent with the strong resonance limit in section 3.2.

3.1. *Quasi-linear (Lorentz') theory*

In order to overcome problems with the nonlinear friction term in (3.1), Lorentz (1922) proposed to replace it by a linear term ru, with effective linear friction coefficient r to be determined. In the case of uniform hypsometry the system (3.1) becomes linear and the response will be of the form $\zeta = |\alpha|\cos(\omega t + \varphi) = \mathrm{Re}[\alpha\,\mathrm{e}^{\mathrm{i}\omega t}]$, where $\alpha = |\alpha|\mathrm{e}^{\mathrm{i}\varphi}$, and con-

sequently $u = -(A_0/O)\,\omega|\alpha|\sin(\omega t + \varphi)$. Lorentz' energy principle states that the energy dissipation per tidal cycle should be the same for both formulae: $\langle ru^2 \rangle = \langle (\tilde{f}/L)\,|u|u^2 \rangle$, in which $\langle \cdot \rangle$ denotes averaging over a tidal cycle. Evaluation of the corresponding integrals leads to

$$r = \nu_0\,\omega|\alpha|, \quad \text{with } \nu_0 = \tfrac{8}{3\pi}\tfrac{\tilde{f}A_0}{OL}, \tag{3.2}$$

i.e. effective friction increases linearly with tidal amplitude in the basin. This leads to the dispersion (frequency response) relation

$$(\omega_0{}^2 - \omega^2)\,\alpha + \mathrm{i}\,\nu_0\,\omega^2\,|\alpha|\alpha = \omega_0{}^2\,\alpha_e, \tag{3.3}$$

which can be solved for the amplification factor to find the frequency response function

$$\frac{|\alpha|}{\alpha_e} = \sqrt{\frac{\sqrt{(1 - (\frac{\omega}{\omega_0})^2)^4 + 4\nu_0{}^2(\frac{\omega}{\omega_0})^4\alpha_e{}^2} - (1 - (\frac{\omega}{\omega_0})^2)^2}{2\nu_0{}^2(\frac{\omega}{\omega_0})^4\alpha_e{}^2}}, \tag{3.4}$$

which can be combined with (3.3) to find the phase lag $\varphi \in (-\pi, 0)$ as well, from $\varphi = \arccos((1 - (\frac{\omega}{\omega_0})^2)\,\frac{|\alpha|}{\alpha_e})$.

3.2. *Weakly nonlinear theory for strong resonance*

Elaborating upon the work of Green (1992), Maas (1997) showed that non-uniform hypsometry $A(\zeta)$ in a Helmholtz basin leads to a reduction of the low tide period and an increase of the high tide period. In order to illustrate the analysis of possible nonlinear effects on the response curves, it will be discussed here as a relatively simple example, although Terra *et al.* (2004*b*) show that the same analysis is applicable to more general basins as well. A mathematical investigation of (3.1) with linearized friction and non-uniform hypsometry was carried out in the small-amplitude strongly resonant limit (Maas & Doelman 2002; Doelman *et al.* 2002). Introducing the asymptotic parameter $\varepsilon \ll 1$ as a measure for the assumption of small amplitudes $\tilde{\zeta} = \mathcal{O}(\varepsilon)$, weak linear friction $\tilde{r} = \mathcal{O}(\varepsilon^2)$ and nearly resonant $\omega = \omega_0(1 + \varepsilon^2\sigma)$ small forcing $\tilde{\zeta}_e = \mathcal{O}(\varepsilon^3)$, where tildes are

used to denote rescaled dimensionless variables (for details, see Maas 1997), a dynamical system was derived by averaging methods describing the (slow) evolution of the response amplitude and phase. In this strongly resonant limit, the resonance peak is high $\mathcal{O}(\varepsilon^{-2})$ and narrow $\mathcal{O}(\varepsilon^2)$. The dispersion relation describing it, after translating their results back to dimensional variables and using the effective friction coefficient r from Lorentz' procedure, is given by

$$(\omega_0 - \omega)\,\alpha + \omega_0\Gamma|\alpha|^2\alpha + \mathrm{i}\,\frac{1}{2}\nu_0\,\omega_0\,|\alpha|\alpha = \frac{1}{2}\omega_0\,\alpha_e, \qquad (3.5)$$

in which $\Gamma = \frac{1}{16A_0}\frac{\mathrm{d}^2 A}{\mathrm{d}\zeta^2}|_0 - \frac{7}{24A_0{}^2}(\frac{\mathrm{d}A}{\mathrm{d}\zeta}|_0)^2$ is a coefficient resulting from the non-uniform hypsometry term. The subscript $|_0$ expresses that the respective value should be calculated for the situation at rest ($\zeta = 0$). Note that (3.5) is applicable to many more processes, see the discussion in section 5.1. The hypsometry term causes the response curve to tilt, see figure 3, because the effective eigenfrequency depends on the amplitude in this case, with $\Gamma|\alpha|^2$ being the relative change of the effective eigenfrequency. As indicated in the figure, this can lead to multiple equilibria: different response regimes are possible under the same forcing conditions. At the indicated forcing frequency (dashed line), with medium forcing amplitude (curve B), three steady states are found, one with relatively high amplification and one with less amplification. The middle one is unstable hence will not occur in practice. Consequently sudden regime changes will occur if the forcing conditions change such that the present branch is not a solution anymore. When conditions subsequently return to the original situation, the system will remain in the newly found regime and does not return to the original response (hysteresis). Moreover, Maas & Doelman (2002); Doelman *et al.* (2002) showed that the regime changes may occur *chaotically* under continuously evolving forcing conditions.

Clearly, there are some major flaws in this picture. For $\omega \downarrow 0$ the amplification factor should tend to 1, because for very slow oscillations the basin and sea simply serve as
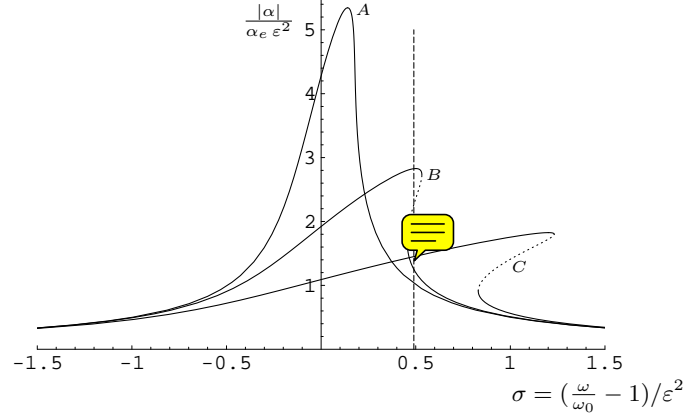
FIGURE 3. Frequency response curves according to (3.5) for fixed friction parameter ν_0 and hypsometry coefficient Γ and increasing forcing amplitudes for curves A, B and C, respectively. Solid curves denote stable branches, the dotted curves are unstable. A dashed vertical line at $\sigma = 0.49$ indicates that multiple equilibria are found under certain conditions.

communicating vessels. However, $\omega = 0$ is not special in (3.5), because of the scaling which is designed to apply near resonance $\omega \simeq \omega_0$. We should consider the limit $\sigma \to -\infty$, in which case the amplification tends to zero, because the weakly nonlinear theory zooms in on an allegedly very high resonance peak $\mathcal{O}(\varepsilon^{-2})$ such that 1 and 0 are indistinguishable in this limit. As a consequence, (3.5) by itself is inadequate to describe the results of the experiments, for which the resonance is not infinitely strong.
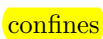
3.3. *Heuristic incorporation of weakly nonlinear limit within quasi-linear theory*

In order to obtain a theory with which the laboratory measurements can be compared, the weakly nonlinear results for the strong resonance limit must be incorporated within the quasi-linear theory for finite amplitude from section 3.1. The combined theory should satisfy the restriction that it *a)* equals (3.3) in the absence of nonlinearity ($\Gamma = 0$), *b)* reduces to (3.5) for $\omega \to \omega_0$, *c)* implies amplification factor $|\alpha|/\alpha_e \to 1$ for $\omega \downarrow 0$ and $|\alpha|/\alpha_e \to 0$ for $\omega \to \infty$.

Dividing (3.3) by $2\omega_0$ one can see (3.5), with $\Gamma = 0$, emerging from (3.3) by taking the limit $\omega \to \omega_0$ except in the difference term $\omega_0 - \omega$. Reverting the process, multiplying
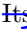
(3.5) by $2\omega_0$ to

$$2\omega_0(\omega_0 - \omega)\,\alpha + 2\omega_0{}^2\Gamma|\alpha|^2\alpha + \mathrm{i}\,\nu_0\,\omega_0{}^2\,|\alpha|\alpha = \omega_0{}^2\,\alpha_e,$$

one regains (3.3) with an additional term $2\omega^2\Gamma|\alpha|^2\alpha$ upon replacing $2\omega_0$, $2\omega_0{}^2\Gamma$ and $\nu_0\omega_0{}^2$ by $\omega_0 + \omega$, $2\omega^2\Gamma$ and $\nu_0\omega^2$ and leaving the right-hand side as it is. Although restriction *a)* confines the finite resonance result for the terms that occur in (3.3) too, the additional 'hypsometry' term could be anything with the correct limiting behaviour for $\omega \to \omega_0$. The restriction *c)* requires the 'hypsometry' term to vanish for $\omega \downarrow 0$. In fact, every combination $2\omega^n\omega_0{}^{2-n}\Gamma|\alpha|^2\alpha$ with $n > 0$ would do, but $n = 1, 2$ are the most likely choices in view of the derivation. Because the resulting equation is more easily solved for ω^2 as a function of $|\alpha|$ if we choose $n = 2$, we use

$$(\omega_0{}^2 - \omega^2)\,\alpha + 2\omega^2\Gamma|\alpha|^2\alpha + \mathrm{i}\,\nu_0\,\omega^2\,|\alpha|\alpha = \omega_0{}^2\,\alpha_e \qquad (3.6)$$

as the simplest combined dispersion relation for finite resonance with nonlinearity. The experimental results in section 4 will be compared with this equation.

4. Results

In this section the response curves for a number of cases with different pipes and basin area are presented. First measurements with full basin area without hypsometry are shown as reference case for which quasi-linear theory (3.3) applies. Next, the influence of non-uniform hypsometry is investigated by introducing artificial 'tidal flats'. Its effect on the response curve appears not to be significant compared to the width of the resonance peak due to friction. Multiple equilibria were found when introducing smooth pipe ends and reducing the basin area in order to reduce the effect of friction and are discussed in section 4.3. The smooth shape of the pipe ends appears to be the key difference in section 4.4 and the section is concluded showing the dependence on the basin area.
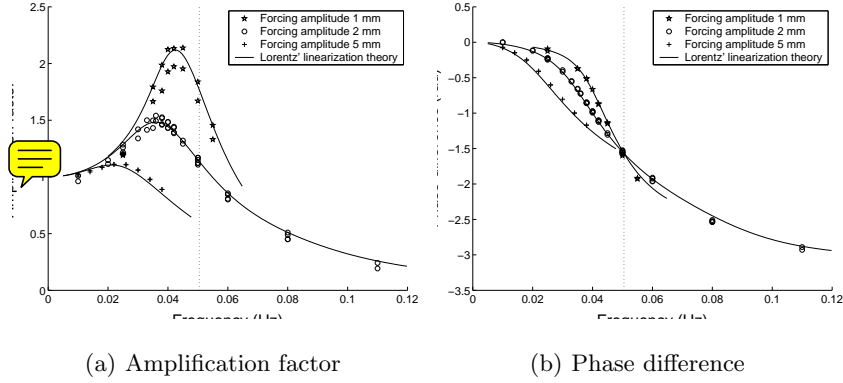
(a) Amplification factor   (b) Phase difference

FIGURE 4. Response curves: amplification factor and phase lag between the tide at sea and in the basin as a function of forcing frequency, for the same configuration as in figure 2. Three series of measurements with forcing amplitudes $\alpha_e \approx 1, 2, 5$ mm are shown, for each of which results for two sensors in the basin have been obtained. Slight amplitude differences between both basin sensors can be noted, in particular at 1 mm forcing amplitude. Solid curves show the fit to Lorentz' theory (3.4). The Helmholtz frequency $\omega_0 = 0.0505$ Hz is indicated by a dotted vertical line. Note that one fit is used to describe all three curves. Apparently the decrease of the resonator's quality is adequately described by Lorentz' linearization theory.

4.1. *Quasi-linear case: straight pipe entrance*

As a reference, measurements were performed with uniform hypsometry, using the full basin area ($A_0 = 0.916$ m^2) with vertical sidewalls and a straight pipe ($L = 441$ mm) with circular cross section ($O = 4.6 \cdot 10^{-3}$ m^2). The quasi-linear theory according to (3.4) has been fitted to the measurements minimizing the least square error in the complex α/α_e-plane. Because the effective pipe length differs from the actual pipe length due to the added mass effect it has to be determined empirically from the apparent eigenfrequency of the basin. The same holds good for the head loss parameter $\tilde{f}$. Therefore, ω_0 and ν_0 are used as fitting parameters. The curves shown in Fig. 4 are for the best fit with $\omega_0 = 50.5\pm0.9\cdot10^{-3}$ Hz $= 0.317\pm0.006$ rad s^{-1}, $\nu_0 = 374\pm9$ m^{-1}. So the effective pipe length $L_{\text{eff}} = 48.9\pm1.7$ cm is 4.8 cm longer than the actual length. Furthermore, $\tilde{f} = 0.97\pm0.02$ has the same order of magnitude as Ito (1970) found for motion on real geophysical scale
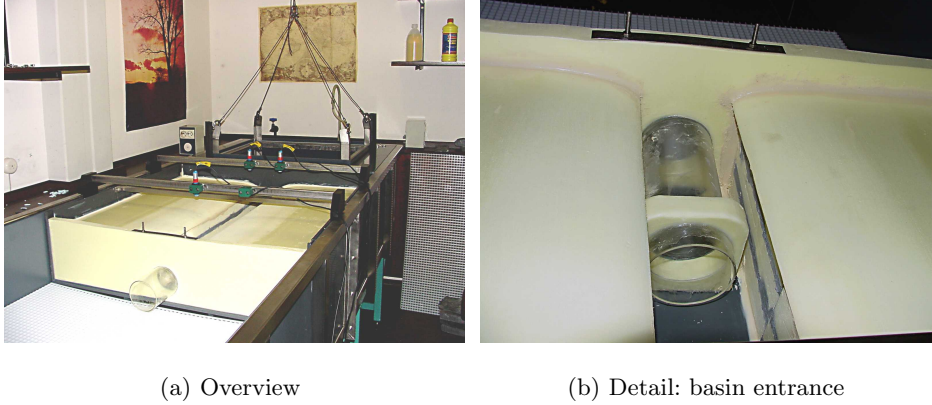
(a) Overview   (b) Detail: basin entrance

FIGURE 5. Pictures of the laboratory basin with 'tidal flats', to the left and right side of the

main channel.

$(f \approx 1.5)$ by comparing the results of his numerical model with tidal data after the partial

closure of the entrance of the Port of Ofunato. Hence our experiments corroborate his

numerical/empirical value. So, although fitting is involved to determine the precise value

of ω_0 and ν_0, they do not differ much from their rough independent estimate. Moreover,

the decrease of the resonator's quality (the height and sharpness of the resonance) due

to increased effective friction with increasing tidal amplitude, is explained well by the

theory. Note that the phase lag is $-\pi/2$ for $\omega = \omega_0$ irrespective of forcing amplitude.

This is in perfect correspondence with quasi-linear theory (3.3), but will be different if

additional nonlinear effects become important in equation (3.6). See Terra *et al.* (2004*a*)

for a more extensive discussion on the validation of Lorentz' linearization procedure.

4.2. *Non-uniform hypsometry*

In order to measure the nonlinear effect of non-uniform hypsometry, artificial 'tidal flats'

were introduced in the basin, see figure 5. The mean tidal curve was constructed by

wrapping the measurements onto a single period subtracting an integer number of tidal

periods (14.3 s in this case) from each time value. Figure 6 clearly shows that the low

tide period decreases and the high tide period increases because water spreads over a
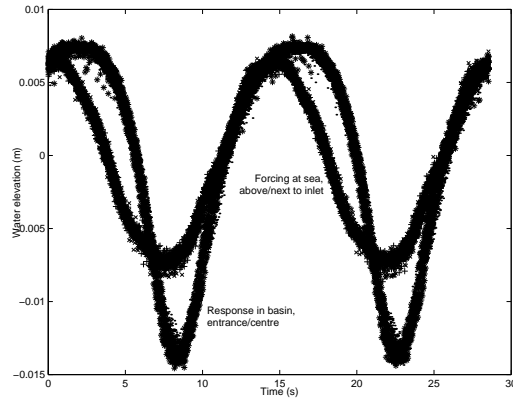
FIGURE 6. Tidal curve of measurements with tidal flats at forcing frequency 0.0700 Hz and forcing amplitude approximately 7 mm. The two curves measured at sea are indistinguishable. The two curves measured at different positions inside the basin are almost the same as well.

smaller or larger basin area, respectively. In principle one would expect this to be visible in the response curves as well, which should get tilted because of the dependence of the effective eigenfrequency on the oscillation's amplitude. However, the response curves for this basin with non-uniform hypsometry do not differ significantly from the ones shown in figure 4 for the basin with vertical sidewalls. The reason is that friction widens the response curves. Possible tilting of the response curves is invisible relative to the frictional width of the peaks.

The effect of non-uniform hypsometry increases if the difference between the basin area at high and low tide is larger, but the effective friction is smaller when tidal ranges are low (cf. section 4.1). Therefore, we tried to maximize the relative effect of hypsometry by decreasing the slope of the 'tidal flat', such that a small change in water level results in a large change in basin area. However, this leads to a number of small scale effects that destroy the uniform nature of the Helmholtz mode: cohesion and adhesion of the water to the slope causes a significant delay when wetting/drying the tidal flat. More importantly, because the water depth is increasingly small over the tidal flat when decreasing its slope,

the tidal wave velocity and wavelength decrease. As a consequence there will be a phase lag between the tidal flat and the deeper part of the basin, contradicting the assumption of uniformity of the Helmholtz mode. This breaks down the model (3.1) and effectively leads to additional damping.

The effects of cohesion and adhesion are not likely to be important in large-scale natural basins. The decrease of the tidal wavelength can indeed be observed in natural tidal flats as well, although its effect may be diminished by the fractal nature of the tidal channel system (Cleveringa & Oost 1999). In fact, this causes the total length of the waterline to be much larger than with a straightforward construction as shown in figure 5. Consequently, the actual slope and in particular the water depth near the waterline need not be that small to achieve large changes in basin area with small changes in water level. From a physical point of view, the gullies transport the water to and from the shoals, hence causing the tide to remain uniform, thus eliminating the damping effect of the phase differences between the sealevel in channels and above shoals.

4.3. *Multiple equilibria*

In order to reduce the effect of friction, the basin area A_0 was reduced† (from 0.916 m^2 to 0.255 m^2) and smooth trumpet-shaped pipe ends (figure 9(b)) were introduced. Both pipe ends of increasing diameter are 145 mm long. With a straight part of 30 mm, 92.9 mm interior diameter, in between the total length of the pipe is 320 mm. Indeed the response curves are much higher and sharper in this case. Actually, although no artificial topography had yet been introduced, multiple equilibria were found. Apparently, another nonlinear effect is at play. A number of processes possibly explaining the observed phenomena, will be discussed in section 5.

† This reduces the amplitude of currents through the pipe. Hence, due to the quadratic dependence of friction on the current, the effective friction decreases.

(a) Amplification factor

(b) Phase difference

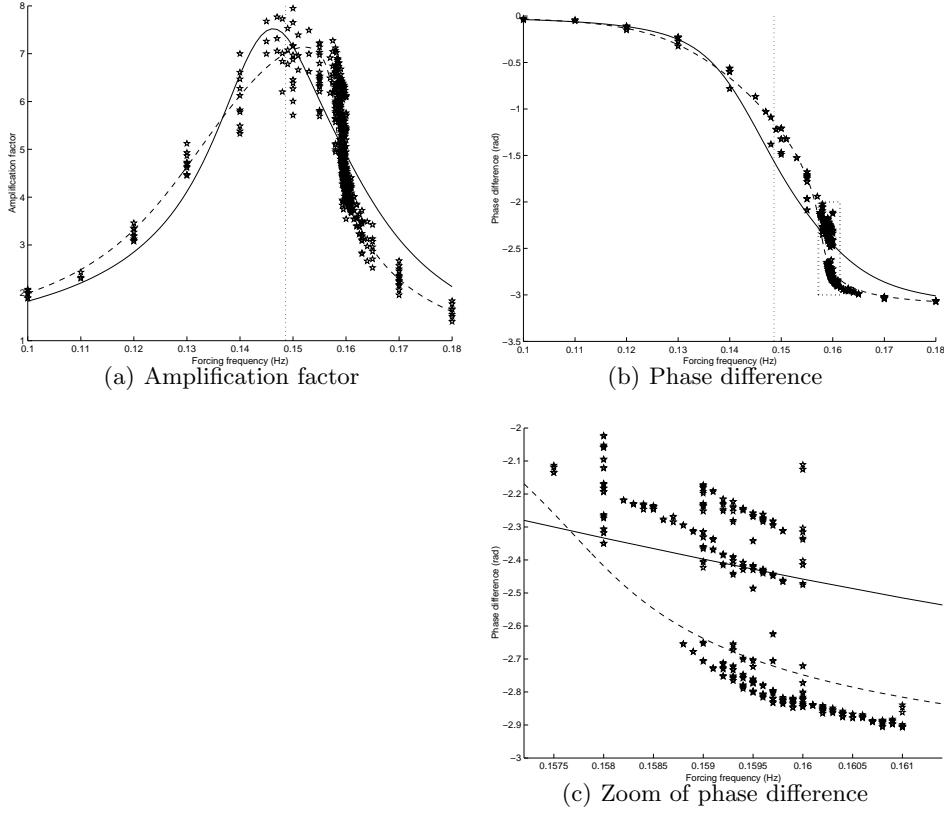
(c) Zoom of phase difference

FIGURE 7. Response curves: amplification factor and phase lag between the tide at sea and in the basin as a function of forcing frequency with forcing amplitude $\alpha_e \approx 1$ mm. Solid curves show the fit to Lorentz' theory (3.4) with parameters $\omega_0 = 0.149$ Hz (indicated by a dotted vertical line) and $\nu_0 = 19.4$ m^{-1}, whereas the dashed curves show the extended nonlinear theory (3.6) with parameters $\omega_0 = 0.140$ Hz, $\nu_0 = 15.1$ m^{-1} and $\Gamma = 1.63 \cdot 10^3$ m^{-2}. Figure 7(c) zooms in on the small frequency range (indicated by the box in figure 7(b)) for which multiple equilibria were found: the upper branch was followed when gradually increasing the forcing frequency, the lower branch corresponds with gradually decreasing frequencies. Because the results for both basin sensors are plotted together, the two branches are less clearly identified in figure 7(a), as the amplitude differences between the two sensor locations are comparable to the gap between the branches.

Figure 7 shows the response curve found under these conditions at 1 mm forcing amplitude. It is different from figure 4 in that this curve tilts to the right. In particular the phase difference deviates from $-\pi/2$ at $\omega = \omega_0$, which is an indication of the influence

of nonlinear effects as well. Indeed the response curve according to Lorentz' linearization theory (solid curve) fits less well in this case, whereas the (dashed) curve corresponding with the extended nonlinear theory (3.6) describes the global behaviour of the response curve much better. Multiple equilibria occur in a small but reproducible frequency range only, see figure 7(c). Note the gap in this figure in which phase differences between -2.6 and -2.5 do not occur because the corresponding branch of steady solutions is unstable. Although ~~the~~ (3.6) does predict multiple equilibria as well for Γ large enough, it apparently does not describe the system well enough to predict the correct parameter range, as it does not predict multiple equilibrium for the value of Γ that best fits the data. This may be caused by the fact that, having been derived from the small-amplitude limit near resonance, it captures the first order correction to the effective eigenfrequency only.

Tantamount to the presence of multiple equilibria is the occurrence of hysteresis: when performing a series of measurements gradually increasing the forcing frequency, the tidal response in the basin remains in the higher amplitude (less phase lag) regime until it 'suddenly' collapses to the lower amplitude branch. Subsequently decreasing the forcing frequency the lower branch is followed until a 'sudden' transition to the higher amplitude regime occurs, see figure 8(a). In this figure only high and low tide measurements are plotted in order to obtain the envelop of the signals oscillating at forcing frequency 0.1592 Hz (6.3 s period). At the start of the time series, the basin response seems to be in the lower amplitude regime in which it started as the forcing frequency had just been decreased from higher values. However, although there is no change in the forcing conditions during the plotted interval the basin response shifts to the higher amplitude regime and remains there (also for long after the plotted part of the time series). Apparently the lower amplitude regime near which the basin started had ceased to exist under these conditions so the system is forced to transfer to the stable higher amplitude regime. The
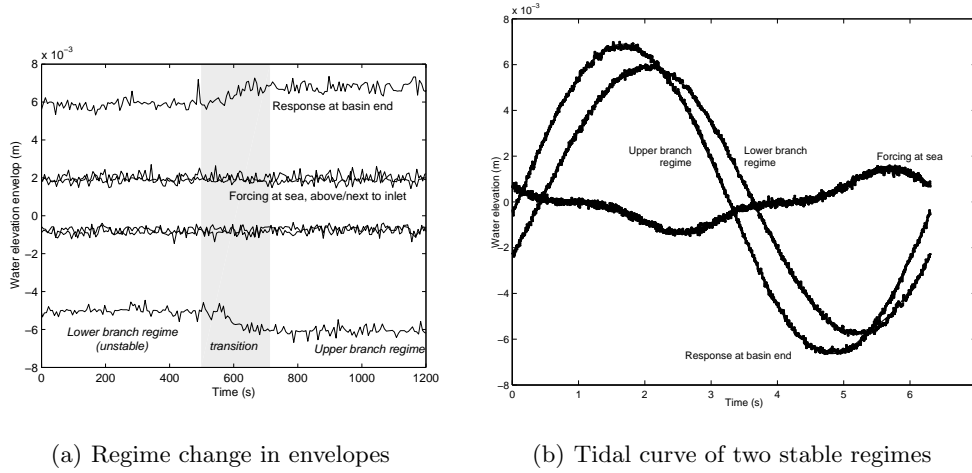
(a) Regime change in envelopes

(b) Tidal curve of two stable regimes

FIGURE 8. Illustrations of multiple equilibria: 8(a) Time series of the envelop of forcing at sea and response in the basin by plotting measurements of high and low tide. The forcing conditions remain at frequency 0.1592 Hz and amplitude 1 mm during the entire time series, but the response shifts to a higher amplitude regime. 8(b) Measured tidal curves of forcing at sea and two different stable response regimes under the very same forcing conditions. Forcing is at 0.1588 Hz frequency, 1 mm amplitude for both cases, but the response has a phase lag of 2.29 rad and amplitudes of 5.5 mm for the higher amplitude regime and a phase lag of 2.65 rad and amplitudes of 5.1–5.8 mm for the lower amplitude regime. Note that overtides are clearly present at sea but do not propagate into the basin.

lower amplitude regime not only has lower amplitude, the phase lag with the forcing at sea is larger as well as can be seen in figure 8(b) which shows two different tidal curves of the response in the basin under the same forcing at sea in a single plot. The response amplitudes can be different only because the phase lag, hence the input of energy, differs. The phase lag is different because the effective eigenfrequency of the basin is different at different tidal amplitudes.

4.4. *Smooth pipe entrance versus straight pipes*

In the previous section we showed the occurrence of multiple equilibria after reducing friction by decreasing the basin area and introducing smooth trumpet-shaped pipe ends.

Because vertical sidewalls were used, non-uniform hypsometry cannot be the mechanism responsible for this effect. Although the reduction of the basin area dramatically decreases effective friction, hence increases amplification, it is not the key factor either (see also section 4.5). Figure 9 shows that the key difference is the shape of the pipe ends: with straight pipe ends no nonlinear effects are observed, the curves for the best quasi-linear Lorentz' fit and the best extended nonlinear fit actually coincide. With smooth trumpet-shaped pipe ends the results clearly deviate from Lorentz' theory and are better described by the nonlinear extension. Apparently, it is the shape of the pipe entrance that causes the effective eigenfrequency to depend on the amplitude. The most likely scenario is that the effective length of the pipe depends on the fluid velocity and turbulent gyres of the flow through the pipe. In that case the first order correction to the quasi-linear dispersion relation (3.3) should lead to the same equation (3.6) as for non-uniform hypsometry. No quantitative analysis to corroborate this description is available yet however.

4.5. *Dependence of resonance characteristics on basin area*

Because of the apparent influence of basin area on the effective friction, a series of measurements at different basin areas have been performed. For this series a pipe with smooth trumpet-shaped ends (like in the previous section) was used. At the basin side it was cut in order to reduce the height of the opening and smoothen the transition to the bottom of the basin. The total pipe length is 340 mm, 2 cm longer than in section 4.3, for technical reasons. Figure 10 shows the response curve parameters fitted to the respective measurements. The eigenfrequency decreases with the square root of basin area A_0 in correspondence with its definition $\omega_0 = \sqrt{gO/(A_0L)}$.

Equation (3.2) suggests a linear relation between the friction parameter ν_0 and A_0. However, figure 10(b) clearly shows a quadratic deviation from linear dependence. Perhaps this is related to statistical interdependence between ν_0 and the tilting parameter

(a) Straight pipe end

(b) Smooth trumpet-shaped pipe end

(c) Amplification factor, straight pipe end

(d) Amplification factor, smooth pipe end

(e) Phase difference, straight pipe end

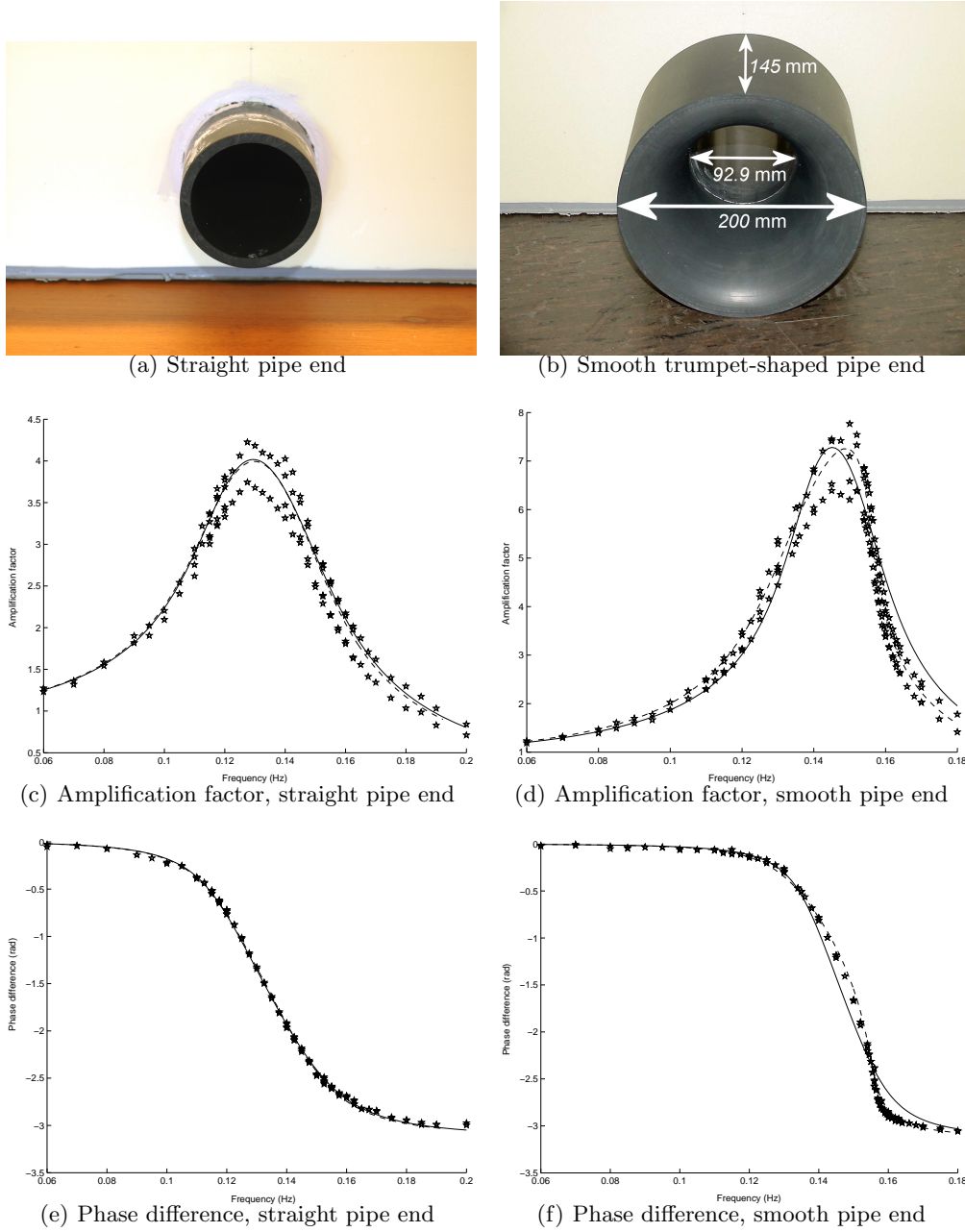(f) Phase difference, smooth pipe end

FIGURE 9. Response curves with and without smooth trumpet-shaped pipe ends. Forcing amplitude $\alpha_e \approx 1$ mm in both cases. The straight pipe (left) is 313 mm long with 92.9 mm inner diameter, the smooth pipe (right) has a total length of 340 mm including 145 mm trumpet-shaped openings at either side, in which the inner diameter increases from 92.9 mm at the interior to 200 mm at the ends. On the basin side, the lower part of the entrance has been cut to better merge with the basin's bottom. Solid curves show the fit to Lorentz' theory (3.4) with parameters $\omega_0 = 0.134$ Hz and $\nu_0 = 62.2$ m^{-1} in the straight pipe case, $\omega_0 = 0.147$ Hz and $\nu_0 = 18.1$ m^{-1} in the smooth entrance case. Dashed curves show the extended nonlinear theory (3.6) with parameters $\omega_0 = 0.133$ Hz, $\nu_0 = 61.1$ m^{-1} and $\Gamma = 0.60 \cdot 10^3$ m^{-2} in the straight pipe case, $\omega_0 = 0.141$ Hz, $\nu_0 = 16.0$ m^{-1} and $\Gamma = 1.08 \cdot 10^3$ m^{-2} in the smooth entrance case. Again amplitude differences within the basin can be seen between the sensors at the end and entrance of the basin respectively.

Γ which, besides tilting, has a damping effect on the response curve as well by detuning forcing and eigenfrequency.

There is no quantitative theory for Γ yet for the Helmholtz mode with uniform hypsometry. From figure 10(c) we conclude that it increases quadratically with A_0. Note that the tilting effect of Γ on the response curve is measured by $\Gamma|\alpha|^2$ in (3.6), so the increase of the friction parameter ν_0 decreasing the response amplitude $|\alpha|$ needs to be considered as well when assessing the importance of the tilting parameter.

For none of the cases in this series of measurements, multiple equilibria were found. For comparison, the parameters ω_0, ν_0 and Γ found for the configuration in section 4.3, for which multiple equilibria were found, are plotted with stars in figure 10 as well. Although ω_0 and Γ were slightly higher in that case (as was expected for the eigenfrequency ω_0 because the pipe was a bit shorter), the friction coefficient was significantly lower in that case, possibly because the care taken in preventing leakage was traded for being able to swiftly change the configuration. Apparently this causes the absence of multiple equilibria in the present series of measurements.

5. Discussion of alternative theories

The results presented in the previous section show that apart from non-uniform hypsometry there must be another process leading to a similar nonlinear effect. In this section a number of such processes are discussed, emphasizing the physical mechanisms rather than mathematical solution. First a number of effects related to the nonlinear character of advection and continuity are considered. The mechanism discussed in section 5.2 shows that the results are not exclusive for shallow water models but may occur in non-hydrostatic models as well. Finally, there is some discussion on different friction regimes as a less likely candidate for explaining the observed phenomena.
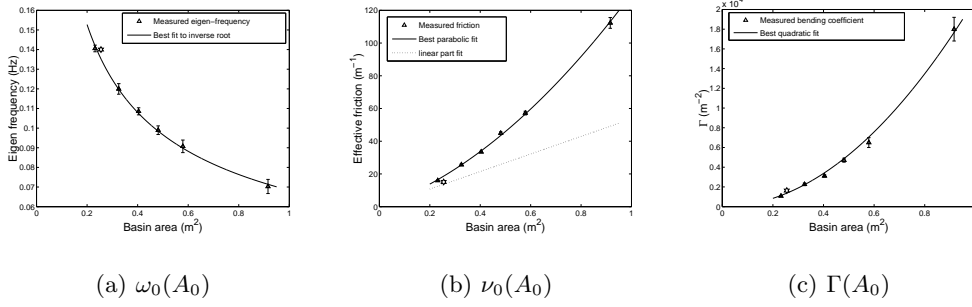
(a) $\omega_0(A_0)$ (b) $\nu_0(A_0)$ (c) $\Gamma(A_0)$

FIGURE 10. Response curve parameters as a function of basin area. Eigenfrequency ω_0 is inversely proportional with the square root of A_0 as expected from its definition just before section 3.1. Although a linear relation between the friction parameter ν_0 and basin area A_0 was expected on the basis of (3.2), it clearly comprises a quadratic deviation from linear dependence. No quantitative theory is available for the nonlinear tilting parameter Γ as yet. It appears to depend on basin area A_0 quadratically. For comparison, six-pointed stars denoting the parameters found in section 4.3, with a slightly different pipe, have been added.

5.1. *Advective and continuity effects*

Apart from friction, there are two nonlinear terms in the two-dimensional depth-averaged **shallow water equations**

$$\frac{\partial \mathbf{U}}{\partial t} + [\mathbf{U} \cdot \nabla]\mathbf{U} = -g\nabla\zeta - \frac{\tau_{\mathbf{b}}}{\rho D}, \tag{5.1a}$$

$$\frac{\partial \zeta}{\partial t} + \nabla \cdot [D\mathbf{U}] = 0, \tag{5.1b}$$

where $\tau_{\mathbf{b}}$ is the bottom friction stress, ρ the density, $\zeta(\mathbf{x}, t), \mathbf{U}(\mathbf{x}, t)$ the sealevel elevation and current at position $\mathbf{x}$, time t and $D = H(\mathbf{x}) + \zeta(\mathbf{x}, t)$ is the total water depth. The advective term $[\mathbf{U} \cdot \nabla]\mathbf{U}$ and the continuity term $\nabla \cdot [\zeta \mathbf{U}]$ not only induce the well-known nonlinear effect of distorting the tidal curve by exciting higher harmonics, but may also change response curves. An extensive calculation for the same strongly resonant limit as in section 3.2 leads to nonlinear amplitude equations of which the Helmholtz results are a special case (Terra *et al.* 2004*b*).

The effects of **non-uniform hypsometry** discussed along the lines of Maas (1997);

Maas & Doelman (2002); Doelman *et al.* (2002) in section 3.2 can be interpreted as a continuity effect, because it is a consequence of the fact that the flux of water through the channel spreads out over a variable wet area of the basin. As a consequence the same current through the channel leads to a different rise in the basin's water level, hence the restoring force of the oscillator, depending on the phase of the tide. At high tide the resulting water level change is less than at low tide.

The opposite effect emerges when considering the influence of water level elevation changes on the cross section of the channel itself (Miles 1981). Indeed at high tide the same current velocities over larger channel cross section leads to larger flux of water through the channel than at low tide when the channel cross section is relatively small. Hence the nonlinear effect caused by the dependence of the **channel cross section** on the water level reduces the high tide period and decreases water level changes at low tide, so this also leads to an equation similar to (3.5).

Actually, (3.5) appears to be the **generic form** of the first-order nonlinear correction to the dispersion relation whenever the effective eigenfrequency depends on amplitude. Apart from explicit derivations for particular mechanisms the main motivation is along the lines of Terra *et al.* (2004*b*): for oscillatory modes ($\omega \neq 0$) the condition for resonant feedback onto itself cannot be fulfilled for triad interactions. The condition for resonant quartic interactions ensures that $|\alpha|^2\alpha$ will generically be the first nonlinear term (see also Nayfeh & Mook 1979, ch. 4). Although this suggests that it is appropriate to use (3.5) to describe the results from our laboratory experiments as well, a proper analytical derivation has not been given yet. In particular, a theoretical value for Γ is not available for this situation.

The results in section 4.4 show that the smooth **trumpet-like shape** of the pipe entrance plays a key role in the occurrence of nonlinear changes to the response curve in

the laboratory setting. Apparently, it too causes the effective eigenfrequency to depend on the amplitude. The most likely mechanism is that the effective pipe length changes because of the influence of the entrance shape on the flow in and out of the channel. With straight pipe ends, a jet of water flows out of the pipe into the adjacent sea at rest. As a result vortices are shed, see Wells & van Heijst (2003), whereas the return flow into the pipe behaves more or less uniformly as potential flow. With smooth trumpet-shaped ends, which blend better with the surrounding water, vortices are diminished though not eliminated. The size and strength of these vortices depend on the velocity through the channel. At low amplitudes the outflow is like potential flow as well, at higher amplitudes a jet still forms. Possibly less water actually takes part in the oscillation in the latter case, hence reducing the added mass effect and increasing the effective eigenfrequency.

Indeed we observe that the occurrence of potential or jet-like outflow seems to coincide with the basin being in the lower or higher amplitude regime respectively. On the other hand, it is not yet proven whether this is consequence or cause. In this respect it would be interesting to see if the diffuse nature of the transition between the two regimes in Wells & van Heijst (2003) is reminiscent of hysteresis. They use the velocity through the channel as a control parameter so hysteresis in their experiments would indicate an intrinsic hysteresis mechanism in the change of flow regimes.

Because jet-formation is a consequence of the advection term, it makes sense to classify this effect under the present subsection as well. This effect of the shape of the pipe end may seem peculiar to the laboratory setting because in reality tidal basins are not connected to sea by pipes. However, funnel-shaped tidal inlets are very common. Probably the processes that occur within the trumpet-shaped pipe ends do apply to funnel-shaped tidal inlets as well.

(a) Current in flood period   (b) Friction law   (c) Effective friction coefficient
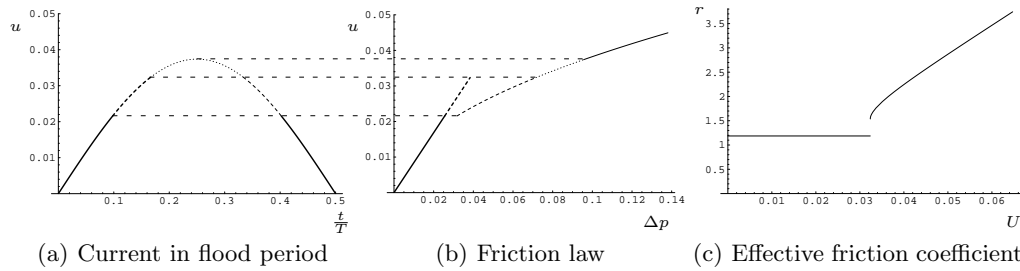
FIGURE 11. Sketch of frictional pressure difference during half a tidal period. 11(b) shows the friction law that was used, with a transition region between the laminar and turbulent regime. In 11(a) the regime of the flow at different intervals during the flood period is indicated. The effective friction coefficient determined from Lorentz' linearization procedure is shown in 11(c).

5.2. *Vertical accelerations*

The continuity and advection effects described in the previous paragraph still play a role in shallow water systems. Another mechanism is feasible if the hydrostatic approximation is abandoned and vertical accelerations are taken into account. As the water level in the basin rises and falls, the distance over which the vertical pressure gradient is induced sustaining the corresponding accelerations, changes as well. Hence the corresponding pressure difference is larger at high tide than at low tide. In other words, inertia increases with water level; consequently the high tide period increases and the low tide period is reduced. A neat and to-the-point treatment of this effect is given by Lorenceau *et al.* (2002), considering oscillations in a liquid column in a partly submerged vertical tube. In fact, Bernoulli (1738) already set out the theory for gravitational oscillations in a U-shaped tube in which this effect plays a role if the two tubes have different cross section. A rough but involved model shows that his equation can also be derived for the present configuration. The resulting estimate for Γ however is orders of magnitudes too low to explain the observed tilting of the resonance curves.

5.3. *Friction regimes*

It is a well-known fact that two regimes have to be distinguished with regard to pipe friction laws. In the laminar regime for low Reynolds numbers $Re = Ud/\nu$, with $U = \omega|\alpha| A_0/O$ the amplitude of the current, d the pipe diameter and $\nu \approx 10^{-6}$ m^2 s^{-1} the viscosity of water, the friction law constitutes a linear increase of the frictional pressure difference with the velocity through the pipe. For high Reynolds numbers $Re \gtrsim 2500$, the flow becomes turbulent and we simplify the discussion by using a quadratic friction law in this regime, rather than one of more sophisticated empirical friction laws (such as Landau & Lifshitz 1959, (43.5)). For the sake of ~~the~~ illustration, suppose the transition even leads to hysteresis, the transition from laminar to turbulent occurring at $Re = 3000$ and from turbulent back to laminar at $Re = 2000$. For the dimensions of the pipe described in section 4.3 for which multiple equilibria were found, this leads to the friction law shown in figure 11(b).

$$\Delta p = \begin{cases} r_0 \, u, & \text{for } u < u_+ \text{ m s}^{-1} \text{ (laminar)} \\ \gamma \, |u|u, & \text{for } u > u_- \text{ m s}^{-1} \text{ (turbulent)} \end{cases} \tag{5.2}$$

with coefficients $r_0 = 1.19, \gamma = 68.4$ and a transition region ranging from $u_- = 0.022$ m s^{-1} to $u_+ = 0.032$ m s^{-1}.

Although the friction laws are derived for stationary flow, we use a quasi-stationary approximation and assume the frictional pressure difference to be given by (5.2) at each stage of the oscillatory tidal flow. If the amplitude of the current is below u_+ the flow remains in the laminar regime, but for higher amplitudes the flow becomes turbulent at maximum flood and maximum ebb, as is illustrated in figure 11. In view of the apparent success of Lorentz' linearization method (Terra *et al.* 2004*a*) we can consequently derive an effective linear friction coefficient as a function of the tidal amplitude according to the energy principle $\langle ru^2 \rangle = \langle \Delta p \, u \rangle$. Performing the integration over the complete tidal

period, this leads to an analytical expression for the effective friction coefficient r. As long as the current amplitude U is below u_+, one simply has $r = r_0 = 1.19$. For U above this upper limit for laminar motion, the expression is much more elaborate. The resulting graph is shown in figure 11(c). Note that in the limit for high amplitude U, the effective friction coefficient r tends to the well-known result $\frac{8}{3\pi}\gamma U$ without taking into account the laminar regime. Next we can solve the resulting linear system to the equivalent of (3.3):

$$|\alpha| = \frac{\omega_0{}^2 \alpha_e}{\sqrt{(\omega_0{}^2 - \omega^2)^2 + r^2\omega^2}} \tag{5.3}$$

in which the effective friction coefficient r depends on $U = A_0/O\,\omega|\alpha|$. Because $|\alpha|$ decreases monotonically as a function of r according to (5.3), multiple equilibria, with two different solutions for the response amplitude $|\alpha|$, are possible only if r decreases as a function of the current amplitude U. Under the quasi-stationary approximation this appears not to be the case.

The transition between friction regimes can be responsible for the observed phenomena only if the quasi-stationary approach used in this section is violated. In that case an *oscillatory pipe friction law* relating the amplitude of the velocity through the pipe (or constriction, in the present situation) to the amplitude of the pressure difference, is needed.

6. Conclusion

Several results of experiments on the response of a co-oscillating tidal resonator have been shown in this paper. The first results in the standard setting with 'large' basin area $A_0 = 0.916$ m^2, uniform hypsometry (i.e. vertical sidewalls) and a straight pipe, corroborate the quasi-linear theory with Lorentz' linearization procedure for quadratic friction. This is an important result by itself, because although Lorentz (1922, 1926)

proposed his linearization scheme at the beginning of the twentieth century already and computations using it on large-scale geophysical tidal systems have been corroborated, ~~no~~ experimental validation has been given ~~so far~~ (see also Terra *et al.* 2004*a*).

Although the introduction of artificial topography ~~in order~~ to simulate the effect of hypsometry did show the influence on the tidal curve, reducing the low tide and increasing the high tide period, tilting of the response curve was found to be insignificant compared to the frictional width of the resonance peak. At the laboratory scale the importance of the hypsometry effect could not be sufficiently increased due to small scale effects. On the other hand, the influence of friction can be reduced by decreasing the basin area and introducing smooth trumpet-shaped pipe ends, the amplification factor of 1.5–2.5 increased to a factor of 8–12. More importantly, a nonlinear effect became significant: tilting of the response curve due to the dependence of the effective eigenfrequency on the amplitude of the tidal oscillation. In particular, under specific conditions multiple equilibria were found: at the same forcing amplitude and frequency two different tidal response regimes could occur in the basin, depending on initial conditions.

These multiple equilibria were found with uniform hypsometry, in which case no nonlinear effects are anticipated based on simple Helmholtz models. In section 5 however, a number of different nonlinear processes are discussed that give rise to similar effects. Terra *et al.* (2004*b*) show that the amplitude equation for the Helmholtz case can be generalized to more general basins with a set of eigenmodes with the nonlinear terms due to advection and continuity in the shallow water equations. The generic nature of the result suggests that a similar derivation can be performed in a three-dimensional setting, needed in order to describe the experimental basin with a pipe connecting the basin to the adjacent 'sea'. The experiments show that the shape of the pipe ends plays a key role in the occurrence of the nonlinear effects. Intuitively this may be related to a depen-

dence of the effective pipe length on the amplitude of the current. In order to explain the experiments, the added mass effect should decrease (for the effective eigenfrequency to increase) with increasing amplitude. However, a quantitative model to compare with the measurements is not available yet.

The apparent importance of the particular three-dimensional shape of the pipe ends used in the experiment may lead to the impression that the occurrence of multiple equilibria is more of an experimental peculiarity. However, two-dimensional funnel-shaped tidal inlets abound in geophysical reality, so the trumpet-shaped pipe ends seem to be more realistic than the straight ones. Moreover, the hypsometry effect is hampered mainly by small scale effects in the laboratory, which leaves the possibility of its relevance for instance in tidal flat systems with their fractal structure of channels (Cleveringa & Oost 1999). Of course truly convincing proof of the relevance of the processes sketched in this paper would lie in finding evidence of these processes in observational records of tidal motion. We think that the results of these experiments provide additional motivation to search for this kind of behaviour in tidal observations. It may be unlikely that sudden changes in the tidal regime and hysteresis, the response of the basin depending not only on the present forcing conditions but also on its history, have been overlooked in the principal tidal components, but they could play a role in secondary undulations. The latter are relatively unimportant for the water level, hence have been investigated less extensively until recently, but their influence on currents can be considerable and reports of irregular behaviour date back to the beginning of the previous century (Honda *et al.* 1908; Nakano 1932). Moreover the results from Maas & Doelman (2002); Doelman *et al.* (2002); Terra *et al.* (2004*b*) suggest to look for internally induced chaotic dynamics of the response amplitudes inside tidal basins without being linked directly to the dynamics

of the forcing, i.e. for variations in harmonic 'constants' (such as reported by Doodson 1924; Gutiérrez *et al.* 1981).

We would like to thank Edwin Keijzer, Theo Kuip, Martin Laan and Sven Ober for their support in designing and constructing the experimental setup and Huib de Swart and Arjen Doelman for carefully reading and commenting on the manuscript.

REFERENCES

BERNOULLI, D. 1738 *Hydrodynamica, sive de viribus et motibus fluidorum commentarii*. Strasbourg: Joh. Reinholdi Dulseckeri, Argentorati.

CLEVERINGA, J. & OOST, A. P. 1999 The fractal geometry of tidal-channel systems in the Dutch Wadden Sea. *Geol & Mijnb* **78** (1), 21–30.

DEFANT, A. 1961 *Physical Oceanography*, , vol. 2. Oxford-London-New York-Paris: Pergamon.

DOELMAN, A., KOENDERINK, A. F. & MAAS, L. R. M. 2002 Quasi-periodically forced nonlinear Helmholtz oscillators. *Physica* D **164**, 1–27.

DOODSON, A. T. 1924 Perturbations on harmonic constants. *Proc. R. Soc. Lond.* A **106**, 513–526.

FRISON, T. W., ABARBANEL, H. D. I., EARLE, M. D., SCHULTZ, J. R. & SCHERER, W. 1999 Chaos and predictability in ocean water levels. *J. Geoph. Res.* **104** (4), 7935–7951.

GALLAGHER, B. S. & MUNK, W. H. 1971 Tides in shallow water: Spectroscopy. *Tellus* pp. 346–363.

GREEN, T. 1992 Liquid oscillations in a basin with varying surface area. *Phys. Fluids* A **4** (3), 630–632.

GUTIÉRREZ, A., MOSETTI, F. & PURGA, N. 1981 On the indetermination of the tidal harmonic constants. *Nuovo Cimento* **4**, 563–575.

HAYASHI, T., KANO, T. & SHIRAI, M. 1966 Hydraulic research on the closely spaced pile breakwater. In *Proc. 10th ASCE Conf. Coastal Eng.*, pp. 873–884.

HONDA, K., TERADA, T., YOSHIDA, Y. & ISITANI, D. 1908 Secondary undulations of oceanic tides. *J. Coll. Sc. Imp. Univ. Tokyo* **24**, 1–113 and 95 plates.

Ito, Y. 1970 Head loss at tsunami-breakwater opening. In *Proc. 12th ASCE Conf. Coastal Eng.*, pp. 2123–2131.

Landau, L. D. & Lifshitz, E. M. 1959 *Fluid Dynamics*, *Course of Theoretical Physics*, vol. 6. Oxford-New York-Toronto-Sydney-Paris-Frankfurt: Pergamon.

LeBlond, P. H. & Mysak, L. A. 1978 *Waves in the Ocean*. Amsterdam-Oxford-New York: Elsevier.

Lorenceau, E., Quéré, D., Ollitrault, J.-Y. & Clanet, C. 2002 Gravitational oscillations of a liquid column in a pipe. *Phys. Fluids* **14** (6), 1985–1992.

Lorentz, H. A. 1922 Het in rekening brengen van den weerstand bij schommelende vloeistof-bewegingen. *De Ingenieur* p. 695, in dutch.

Lorentz, H. A. 1926 *Verslag Staatscommissie Zuiderzee 1918-1926*. Den Haag: Alg. Lands-drukkerij, (in dutch, report senate committee Zuiderzee).

Maas, L. R. M. 1997 On the nonlinear Helmholtz response of almost-enclosed tidal basins with sloping bottoms. *J. Fluid Mech.* **349**, 361–380.

Maas, L. R. M. & Doelman, A. 2002 Chaotic tides. *J. Phys. Oc.* **32** (3), 870–890.

Mei, C. C., Liu, P. L.-F. & Ippen, A. T. 1974 Quadratic loss and scattering of long waves. *J. Waterways, Harbors and Coastal Eng. Div.* **100**, 217–239.

Miles, J. W. 1971 Resonant response of harbors: An equivalent-circuit analysis. *J. Fluid Mech.* **46**, 241–265.

Miles, J. W. 1981 Nonlinear Helmholtz oscillations in harbours and coupled basins. *J. Fluid Mech.* **104**, 407–418.

Nakano, M. 1932 Preliminary note on the accumulation and dissipation of energy of the secondary undulations in a bay. *Proc. Phys.-Math. Soc. Japan* **14**, 44–56.

Nayfeh, A. H. & Mook, D. T. 1979 Pure and applied mathematics. In *Nonlinear oscillations* (ed. L. Bers, P. Hilton & H. Hochstadt), *a Wiley-Interscience series of texts, monographs and tracts* , p. 704. John Wiley & Sons.

Parker, B. B. 1991*a* The relative importance of the various nonlinear mechanisms in a wide range of tidal interactions(review). In *Tidal Hydrodynamics* (ed. B. B. Parker), pp. 237–268. New York: John Wiley & Sons.

PARKER, B. B., ed. 1991*b Tidal Hydrodynamics*, New York. John Wiley & Sons.

RAICHLEN, F. 1966 Harbor resonance. In *Estuary and coastline hydrodynamics* (ed. A. T. Ippen), pp. 281–340. New York: McGraw-Hill.

RAICHLEN, F. & IPPEN, A. T. 1965 Wave induced oscillations in harbors. *J. Hydraulics Div.* pp. 1–26, proceedings of the American Society of Civil Engineers.

TERRA, G. M., VAN DE BERG, W. J. & MAAS, L. R. M. 2004*a* Experimental verification of Lorentz' linearization procedure for quadratic friction. *Fluid Dyn. Res.* Submitted.

TERRA, G. M., DOELMAN, A. & MAAS, L. R. M. 2004*b* Weakly nonlinear cubic interactions in coastal resonance. *J. Fluid Mech.* **520**, 93–134.

TERRETT, F. L., OSORIO, J. D. C. & LEAN, G. H. 1968 Model studies of a perforated breakwater. In *Proc. 11th ASCE Conf. Coastal Eng.*, pp. 1104–1109.

VITTORI, G. 1992 On the chaotic structure of tide elevation in the Lagoon of Venice. In *Proceedings of the 23rd International Conference on Coastal Engineering*, pp. 1826–1839. Venice.

WELLS, M. G. & VAN HEIJST, G.-J. F. 2003 A model of tidal flushing of an estuary by dipole formation. *Dynamics of Atmospheres and Oceans* **37**, 223–244.